

Experimental study of convective condensation in an inclined smooth tube. Part I: Inclination effect on flow pattern and heat transfer coefficient

Stéphane Lips, Josua P. Meyer*

Department of Mechanical and Aeronautical Engineering, University of Pretoria, Pretoria, Private Box X20, Hatfield, 0028, South Africa

Keywords:

Condensation

Inclination angle

Flow pattern

Heat transfer coefficient

ABSTRACT

An experimental study of convective condensation of R134a in an 8.38 mm inner diameter smooth tube in inclined orientations is presented. This article, being the first of a two-part paper (the second part concentrates on the pressure drops and void fractions), presents flow patterns and heat transfer coefficients during condensation for different mass fluxes and vapour qualities for the whole range of inclination angles (from vertical downwards to vertical upwards). The results were compared with three flow pattern maps available in literature. It was found that for low mass fluxes and/or low vapour qualities, the flow pattern is strongly dependent on the inclination angle whereas it remains annular for high mass fluxes and high vapour qualities, whatever the tube orientation. The models of flow pattern maps available in the literature did not predict the experimental data well. In the inclination-dependent zone, experiments showed that there is an optimum inclination angle that leads to the highest heat transfer coefficient for downward flow. The heat transfer coefficient is strongly affected by the liquid and vapour distributions and especially by the liquid thickness at the bottom of the tube for stratified flows. Thus developing a mechanistic model of flow pattern maps is the first step in achieving a predictive tool for the heat transfer coefficient in convective condensation in inclined tubes.

* Corresponding author. Tel.: +27 (0)12 420 3104; Fax: +27 (0)12 362 5124
E-mail address: josua.meyer@up.ac.za

Nomenclature

A	Area (m ²)		
d	Tube diameter of test condenser (m)	Cu	Copper
EB	Energy balance (-)	i	Inner
G	Mass flux (kg/m ² s)	in	Inlet
h	Enthalpy (J/kg)	j	Measurement location
I	Inclination effect (-)	l	Liquid
k	Thermal conductivity (W/mK)	out	Outlet
L	Length of the test condenser (m)	o	Outer
\dot{m}	Mass flow (kg/s)	pre	Pre-condenser
Q	Heat transfer rate (W)	sat	Saturation
R	Thermal resistance (K/W)	ref	Refrigerant
T	Temperature (K)	$test$	Test condenser
x	Vapour quality (-)	v	Vapour
z	Axial direction (m)	w	Wall

Greek symbols

α_{cond}	Heat transfer coefficient (W/m ² K)
β	Inclination angle (>0: upward) (rad)

1. Introduction

Convective condensation occurs in many industrial applications such as air-conditioning, refrigeration, automotive and process industries. Increasing the condenser efficiency in these applications saves space and material and limits the refrigerant load. Higher efficiencies of these systems also reduce the running cost and environmental impact.

Convective condensation in horizontal smooth and enhanced tubes [1-4] has been widely studied and reviewed in the past. However, Lips and Meyer [5] showed in a previous paper that only a few studies deal with condensation in inclined tubes. Some of them are dedicated to the study of thermosyphons or reflux condensers [6,7]. In these systems, vapour and liquid are flowing upwards and downwards respectively. It appears that there is an optimal inclination angle, found to be in the range of 30-45°, which leads to the highest heat transfer coefficients.

An inclination effect on heat transfer coefficients during convective condensation was first noticed by Chato [8]. For downward flows in slightly inclined tubes, increasing the inclination increased the heat transfer coefficient because of the decrease of the liquid depth in the tube. More recently, Wang and Du [9] conducted a theoretical and experimental study on laminar film-wise condensation of steam in small inclined tubes (downward flow in tubes with inner diameter between 1.94 and 4.98 mm). They found that the heat transfer coefficients can be increased or decreased when the tube is tilted, depending on the tube diameter, the vapour quality and the mass flux. They explained their results as the effect of the gravity on the thickness of the liquid film. They developed

an analytical model to predict the shape of the liquid-vapour interface for a stratified flow pattern and compared their model in terms of heat transfer coefficients with experimental results. The deviations were within a range of -28 to + 20%.

Würfel et al. [10] presented an experimental study of two-phase flows inside a 20 mm inner diameter inclined tube. They measured the heat transfer coefficients during condensation of n-heptane in downward flows. They concluded that the heat transfer coefficients increased continuously with increasing inclinations and they developed a correlation taking into account the inclination angle. According to this correlation, an inclination angle of 35° and one of 90° increased the heat transfer coefficient with 10% and 16% respectively, compared with the horizontal orientation.

Akhavan-Behabadi et al. [11] studied experimentally the effect of the inclination angle of an 8.92 mm inner diameter microfin tube for condensing flow of R134a. They found that the heat transfer coefficients were higher for downward flows than for upward flows. During their experiments, they found that the inclination angle that led to the highest heat transfer coefficient was 30° downwards. They developed a correlation based on their experimental data.

The different authors explained that the heat transfer coefficients depend on the distribution of the two phases inside the tube. Thus a study of the flow patterns during convective condensation in inclined tubes is required. Nitheanandan and Soliman [12] conducted an experimental study of the effect of the tube inclination on the flow regime boundaries during condensation of steam. They used a 13.8 mm inner diameter copper tube with small angles of inclination (from 10° downwards to 10° upwards). The range of mass fluxes was 20-280 kg/m²s. They found that the influence of the angle of inclination on the annular flow regime boundary was almost insignificant. However, even a small inclination angle has a strong influence on wavy and slug flow regime boundaries. In a following article [13], they proposed a mechanistic model to predict the transition between stratified and non-stratified flow in their experiments.

Wang et al. [14] carried out an experimental study of the flow pattern transitions during condensation of R11 in a 6 mm inner diameter tube for the whole range of inclination angles. The mass fluxes ranged from 9 to 123.2 kg/m²s. The authors described the different flow patterns present as a function of the inclination angle and proposed some correlations for the transition characteristics.

As a conclusion, we can note that the inclination effect depends strongly on the mass flux, vapour quality and flow pattern. However, the experimental studies on flow patterns and heat transfer coefficients during convective condensation in inclined tubes are strongly limited in terms of experimental conditions. Thus, more experimental studies are necessary to achieve a good understanding of this kind of flow and to develop predictive tools.

This article presents some experimental results obtained during the convective condensation of R134a in an inclined smooth tube. The first part is dedicated to the description of the experimental set-up and the experimental procedure. In the second part, the experimental results are presented, in

terms of flow pattern maps and heat transfer coefficients for different experimental conditions (the varying parameters being the vapour quality, the mass flux and the inclination angle). A comparison of the results with predictions from different models available in the literature is also presented. This paper is part of a two-part paper and focuses on the heat transfer, while the second paper [15] focuses on the pressure drops and void fractions.

2. Experimental set-up

The experimental facility used in this study was adapted from the one already presented in previous work [16,17], and is therefore only briefly described. The set-up consisted of a vapour-compression cycle circulating the refrigerant R134a with a nominal cooling capacity of 10 kW and with two high-pressure condensation lines: the test line and the bypass line (Fig. 1). Each line had its own electronic expansion valve (EEV). The bypass line was used to control the mass flow through the test line and the test pressure and temperature. The bypass line had one water-cooled heat exchanger whereas the test line was constituted by three water-cooled condensers: a pre-condenser, to control the inlet vapour quality, the test condenser, where the measurements were performed, and the post-condenser, to ensure that the fluid is fully liquid before the EEV. After the EEVs, the lines combined and entered a water-heated evaporator, followed by a suction accumulator and a scroll compressor.

The test condenser consisted of a tube-in-tube counterflow heat exchanger, with water in the annulus and refrigerant on the inside. Its length was $L = 1\,488 \pm 3$ mm and the inside channel was a copper tube with an inner diameter of $d_i = 8.38$ mm. Cylindrical sight glasses were positioned at the inlet and outlet of the test condenser. They permitted flow visualisation and acted as insulators against axial heat conduction. The glass tube was chosen carefully to have the same inner diameter as the copper tube. The copper tube was connected to the glass tube with a brass housing and a Teflon U-seal to avoid any disturbance of the flow. A high-speed camera (200 fps) was used to record the flow at the exit of the sight glass. On each side of the test section, three pressure taps were inserted between the sight glasses and the test section. A bush was installed over the outside of the tube and was soldered at both ends. It had three fittings into which the capillary tubes could slide and be soldered. It ensured that the size of the taps was not too large and eased the pressure transducer and capillary piping installation. On each side, two of the pressure taps were connected to two different Gems Sensor pressure transducers for the measurements of the refrigerant absolute pressures at the inlet and outlet of the test section. The two remaining pressure taps were connected to an FP2000 Sensotec differential pressure transducer. The distance between the two pressure taps was 1 704 mm. Straight calming sections were positioned before and after the sight glasses. They were 500 mm and 400 mm long respectively and ensured that the flow was fully developed at the inlet of the test condenser and also minimised disturbance of the exit sight glass. The test condenser could be inclined from 90° upwards to 90° downwards by using flexible hoses at the inlet and outlet of the test section. The outer-wall

temperature of the inner tube of the test condenser was measured at seven stations, equally spaced. At each station, four holes were drilled on the outside of the inner tube at the bottom, the top and the sides of the tube respectively. In each hole, a thermocouple was placed and soldered. Thermocouples wires went of the test section through T-junctions placed regularly on the outer tube. The refrigerant temperatures were taken at four stations: inlet and outlet of the test section, inlet of the pre-condenser and outlet of the post-condenser. These measurements were taken on the outside of the refrigerant tube. At each station, thermocouple measurements were taken with four T-type thermocouples, equally spaced and soldered onto the tube perimeter. At the inlet and outlet of the test section, the consistency was checked between the refrigerant saturation temperature measured by the thermocouples and the saturation temperature determined with the absolute pressure sensors. On the water side, the water temperature was measured at six stations: the inlet and outlet of the pre-, test (i.e. test condenser) and post-condenser. At each station, thermocouple measurements were taken with three T-type thermocouples, equally spaced and soldered onto the tube perimeter. The temperature measurements were made on an adiabatic and insulated copper tube separated from the test-section with a 10 cm long plastic tube. The mixing of the water with a swirler was sufficient to ensure an accurate bulk temperature measurement. All the thermocouples were calibrated together to an accuracy of 0.1°C. The refrigerant and water mass flows through the pre-, test and post-condensers were measured with Coriolis mass flow meters.

3. Data reduction and experimental procedure

Steady-state conditions were assumed when the energy balance (Eq. (1)) was less than 3%, and the temperatures, pressures and mass flows of the system were considered as constant. The temperature stabilization was the limiting parameter and the criterion used was a variation of the mean wall temperature lower than 0.1 K for 10 minutes. Note that a good energy balance ensures that the heat losses to the surroundings are low compared to the heat transfer rates in the three condensers. It also ensures that the temperature measurements are correct on both the refrigerant and water sides. It was unfortunately not possible to check the energy balance for each condenser separately and *a fortiori* for the test condenser. However, it is reasonable to assume that the heat losses are roughly homogeneous in the three condensers. The fluctuation of the measurements and other calculated properties were statistical monitored for stability.

$$EB = \frac{|Q_{ref} - Q_{water}|}{Q_{ref}} \quad (1)$$

The properties of the refrigerant at the inlet of the pre-condenser and the outlet of the post-condenser were determined by temperature and pressure measurements. From these measurements, the thermophysical properties of the condensing refrigerant were determined by utilising data from a refrigerant property database [18]. The heat transfer rate of the refrigerant was determined from the

mass flow rate and change in enthalpy between the inlet of the pre-condenser and the outlet of the post-condenser. The heat transfer rate on the water side was obtained from the mass flow rates of the water in the three condensers and the average inlet and outlet temperatures at the inlet and outlet of the condensers.

The inlet vapour quality x_{in} of the test condenser was calculated from the enthalpy of the refrigerant at the inlet of the test condenser $h_{test,in}$ and the enthalpy of the liquid h_l and the vapour h_v at the same temperature and pressure:

$$x_{in} = \frac{h_{test,in} - h_l}{h_v - h_l} \quad (2)$$

The enthalpy of the refrigerant at the inlet of the test condenser $h_{test,in}$ was calculated from the enthalpy of the refrigerant at the inlet of the pre-condenser $h_{pre,in}$ (calculated from the pressure and the temperature at the inlet of the pre-condenser), the mass flow of the refrigerant \dot{m}_{ref} and the heat transfer rate in the pre-condenser Q_{pre} :

$$h_{test,in} = h_{pre,in} - \frac{|Q_{pre}|}{\dot{m}_{ref}} \quad (3)$$

The heat transfer rate through the pre-condenser was calculated from the water mass flow, specific heat capacity and water temperatures at the inlet and outlet. The vapour quality at the exit of the test section was also calculated from Eq. (2) except that the enthalpy at the outlet of the test condenser was used instead of the inlet enthalpy, calculated as:

$$h_{test,out} = h_{test,in} - \frac{|Q_{test}|}{\dot{m}_{ref}} \quad (4)$$

The heat transfer rate through the test condenser was calculated from the water mass flow, specific heat capacity and water temperatures at the inlet and outlet. The average vapour quality of the test section was calculated by doing the arithmetic mean of the inlet and outlet vapour qualities: $x = (x_{in} + x_{out})/2$. The heat transfer coefficient α_{cond} was calculated by re-arranging Newton's law for condensation considering a constant heat transfer coefficient in the test condenser:

$$\alpha_{cond} = \left| \frac{Q_{test}}{A(\overline{T}_{w,i} - T_{sat})} \right| \quad (5)$$

where A is the area of the inner surface of the test condenser inner tube. T_{sat} is the mean saturation temperature of the refrigerant in the test condenser and was obtained by averaging the saturation temperature measured at the inlet and outlet of the test condenser. $\overline{T}_{w,i}$ is the mean inner-wall temperature. It is linked to the mean outer-wall temperature of the tube, $\overline{T}_{w,o}$, through the thermal resistance of the wall of the copper tube, R_w :

$$\overline{T}_{w,i} = \overline{T}_{w,o} + |Q_{test}R_w| \quad (6)$$

with $R_w = \ln(d_o/d_i)/2\pi k_{Cu}L$.

$\overline{T}_{w,o}$ was calculated by averaging the outer-wall temperature $T_{w,o}^j$ measured at the seven different stations along the test condenser by means of a trapezoidal numerical integration method:

$$\overline{T_{w,o}} = \frac{1}{L} \sum_{j=1}^6 \left[\left(\frac{T_{w,o}^j + T_{w,o}^{j+1}}{2} \right) (z_{j+1} - z_j) \right] \quad (7)$$

where z_j is the j^{th} measurement location along the test condenser.

The experimental set-up does not allow the determination of the local heat transfer coefficient. Averaging the wall and saturation temperature leads to smoothing the variation of the heat transfer coefficient with the vapour quality (that varies between 3.4 % and 11 % across the test-section), with the temperature difference between the wall and the fluid at saturation (that varies with a few Kelvin because of the water temperature variation on the annulus) and with the position on the tube (the wall temperature difference is about 0.2 K between the top and the bottom of the tube). It also hides the saturation temperature variation due to the pressure drop (typically 0.5 K across the test-section). However, the average heat transfer coefficient on the test-section is a characteristic parameter of the flow and can be studied and compared to correlations.

The experiments were conducted for different mass fluxes G , mean vapour qualities x and inclination angles β . The average saturation temperature was kept constant at 40°C and for all the experiments the heat transfer rate in the test condenser was kept constant at $Q_{\text{test}} = 200$ W by changing the mass flow rate of the water. This heat transfer rate led to a maximum vapour quality difference across the test condenser of 0.11 for the lowest mass flux ($G = 200$ kg/m²s) to 0.034 for the highest mass flux ($G = 600$ kg/m²s). Fig. 2 summarises the matrix of the 13 experimental conditions (mass flux and vapour quality) on the Thome-El Hajal-Cavallini [19] flow pattern map. For a horizontal orientation, the experimental conditions mainly correspond to intermittent and annular flow patterns at the boundary of the stratified flow regime.

For each experimental condition, the heat transfer coefficient was determined and the flow pattern was visualised for different inclination angles from 90° upwards to 90° downwards. Table 1 summarises the range of the experimental parameters and their fluctuations. The fluctuations represent the range of variation of the parameter for a certain mass flux and vapour quality and for different angles of inclination. After steady-state conditions were assumed to be reached, the different sensor signals were recorded continuously over a period of five minutes (200 points). To avoid any noise measurement, the average of the points was used for the calculation of the fluid properties and the heat transfer coefficients. The experimental uncertainties of the heat transfer coefficients were calculated using the method of propagation of the errors applied to Eq. (5). The main part of the uncertainty came from the temperature measurements on the water side for the heat transfer rate uncertainty and on the refrigerant sides for saturation and wall temperature uncertainties. The uncertainties on the averaged temperature measurement were estimated to be 0.1 K for each station on both the refrigerant and temperature sides. It led to an uncertainty of the temperature difference of condensation $\overline{T_{w,l}} - T_{\text{sat}}$ slightly lower to 0.1 K due to the propagation of the errors for the summations and averaging. Uncertainties induced by the mass flow meters were negligible. Depending on the experimental

conditions, the relative uncertainties of the heat transfer coefficients were found to be between 4% and 9%. The experimental uncertainty of the vapour quality is directly linked to the energy balance and is lower than 0.03, which is also lower than the vapour quality variation across the test section.

4. Effect of inclination angle on flow patterns

4.1. Experimental flow visualisation

Except for the recordings made by the high-speed video camera, visual observations were also made. However, no uniform flow pattern identification procedure exists at present and the definition of the flow patterns changes from one author to another. For the present study, five flow patterns have been identified: stratified-wavy, annular-wavy, annular, intermittent and churn. This classification is based on that of Kim and Ghajar [20]. Even if this classification was developed for air-water flow, the same types of flow pattern were observed with R134a. Churn flow pattern regroups the flow patterns named bubbly/slug and annular/bubbly/slug by Kim and Ghajar. Smooth stratified and plug flows have not been encountered during the experiments. Intermittent flows regroup slug and plug flows. In the present paper, churn flow is not included in intermittent flow because it appears only for vertical and near vertical orientations.

Fig. 3 summarises the different types of flow patterns considered in this study. It represents a concatenation of a small part of several photos recorded in a short period of time. Thus, it is both a spatial and temporal image of the flow pattern. The time length of the sequences in Fig. 3 is 0.15 s. The flow is stratified-wavy (Fig. 3a) when the liquid is mostly located at the bottom of the tube. Waves occur at the liquid-vapour interface and a thin liquid film can be located at the top of the tube, with small ripples or without. The annular-wavy flow (Fig. 3b) occurs when the thickness of the liquid film at the top of the tube increases: small waves can be present at the surface of this liquid film, but the main part of the liquid is still located at the bottom of the tube. The intermittent flow (Fig. 3c) occurs when the waves in the bottom part of the tube are big enough to reach the top of the tube. The flow is annular (Fig. 3d) when the liquid is located uniformly at the perimeter of the tube and the vapour flows in the tube central core. The churn flow (Fig. 3e) is a highly turbulent flow where slugs of liquid regularly collapse in the central vapour core, leading to dispersed bubbles in the tail of the slugs.

Flow pattern is the result of a balance between gravitational, frictional and capillary forces. Thus it depends on the fluid properties, the mass flux and the vapour quality, but also on the inclination angle of the tube. Fig. 4 shows some photos of the flow for different vapour qualities and different angles of inclination for a mass flux of 300 kg/m²s. An angle of -90° is for vertical flow downwards, 0° is for horizontal flow and +90° is for vertical flow upwards. For high vapour qualities, the flow becomes more and more annular and is insensitive to the inclination angle. For low vapour

qualities, the flow is highly sensitive to the angle of inclination. Stratified flow occurs for slightly downward orientations (negative angles in Fig. 4). For higher inclination angle, intermittent flow is present, whatever the direction of the flow and we observe churn flows for the downward and upward vertical orientations.

Fig. 5 represents the effect of the inclination angle for a constant vapour quality ($x = 0.5$) and for different mass fluxes. For low mass fluxes, the flow pattern is dependent on the inclination angle but for high mass fluxes, the flow is annular, whatever the tube orientation. To conclude, the inclination effect is strongly dependent on both the mass flux and the vapour quality.

4.2. Comparison with Thome-El Hajal-Cavallini flow pattern map [19] for horizontal orientation.

El Hajal et al. [19] proposed a widely used flow pattern map for convective condensation in horizontal tubes. Fig. 6 represents the comparison of the experimental results and our observations of the flow regimes with the Thome-El Hajal-Cavallini flow pattern map [19] for the horizontal orientation. Considering that the experimental points are close to the transitions between the different flow patterns, a good agreement is found between the experimental data and the Thome-El Hajal-Cavallini flow pattern map.

4.3. Comparison with flow pattern maps for inclined orientations.

Several flow pattern maps for two-phase flows in inclined tubes have been published in the literature. It is interesting to compare their prediction with the experimental results obtained with condensing R134a.

The Barnea [21] flow pattern map is a mechanistic model that aims to predict the transitions between smooth-stratified (SS), stratified-wavy (SW), annular (A), churn (Ch), slug (Sl), bubbly (B), elongated bubbly (EB) and dispersed bubbly (DB) flow patterns for the whole range of inclination angles. However, in order to simplify the map, we considered in this study only the distinction between stratified ($S = SS + SW$), annular (A) and intermittent ($I = Ch + Sl + B + EB + DB$) flows. The Barnea [21] flow pattern map has to be built pixel by pixel thanks to a logical path proposed by the author. Fig. 7 shows a comparison of our experimental flow patterns with the Barnea [21] flow pattern map for different angles of inclination. The Barnea [21] flow pattern map was developed for adiabatic air-water flows and it appears that it fails to predict the flow pattern during the condensation of R134a in an 8.38 inner diameter tube: for downward flows, the model underestimates the mass flux that leads to the transition from stratified to annular flow regimes. For upward flows, a better agreement is observed but more experiments are required to estimate the accuracy of the model.

A second flow pattern map available in the literature is that of Crawford et al. [22,23]. In their map, transitions between annular (An), intermittent (I), bubbly (B) and stratified (S) flows are predicted for adiabatic flow of R113 in 25 mm and 38 mm inner diameter tubes. Fig. 8 shows a comparison of experimental flow patterns with the Crawford et al. flow pattern map for different

inclination angles. A relatively good agreement is found between the experiments and the theoretical flow pattern map for the annular transition. However, the predictions in terms of stratified/intermittent transition do not reflect the experiments. No bubbly flow has been observed during the experiments but according to the Crawford et al. flow pattern map, this kind of flow pattern occurs only for very low vapour qualities.

In conclusion, more experiments are necessary to estimate the accuracy of flow pattern maps as a function of the inclination angles presented in the literature. These maps were developed for adiabatic flow and thus do not take into account the condensation phenomenon. However, we can certainly say that the Barnea [21] flow pattern map obviously needs to be adapted for refrigerant flows, whose properties differ strongly from air-water flows. A more comprehensive experimental database is required to build a flow pattern map dedicated specifically to condensing refrigerants in inclined tubes and the Crawford et al. flow pattern map can be a good start to reach this objective.

5. Effect of inclination angle on heat transfer coefficients

The condensation heat transfer coefficient in the test section was measured for a range of mass fluxes and inclination angles. Fig. 9 shows the comparison of experimental results obtained for the horizontal orientation with three different correlations available in the literature. The correlation of Thome et al. [24] comes from a flow pattern-based model. The Cavallini et al. [25] correlation is based on two different regimes, depending on whether the heat transfer coefficient is dependent on the condensation heat flux (ΔT -dependent regime) or not (ΔT -independent flow regime). These two correlations were developed for convective condensation in horizontal tubes only. The correlation of Shah [26] aims to predict the heat transfer coefficient, whatever the tube orientation. A relatively good agreement is observed between the experimental results and the prediction of the correlations, even if the correlations overestimate the experimental data by about 25%.

Some correlations were developed for vertical flows. The correlation of Shah [26] and the correlation of Dobson and Chato [27] were developed for annular flow regimes and are thus independent of the tube orientations. Fig. 10 and Fig. 11 compare the experimental results and the correlations of Shah [26] and Dobson and Chato [27] for upward vertical and downward vertical orientation respectively. The correlations overestimate the data by about 25%, which is the same as that for the horizontal orientation. This deviation may be partially explained by the presence of oil in the refrigerant that tends to decrease the heat transfer coefficient in the condenser. According to previous studies [16,17] performed on the experimental set-up, the amount of oil can be estimated between 0.5 % and 3%. Another cause of the deviation can come from the temperature measurement uncertainties (especially on the water side because of the low water velocities) and the correlation uncertainties. However, the similarity between the comparisons in horizontal and vertical orientation explains why very few studies have been conducted on the heat transfer in inclined tubes: the

difference in terms of heat transfer coefficients between the two types of orientations is lower than the accuracy of the correlations and the discrepancy between the experimental results.

The thermal resistance in a condensation process is mainly induced by the thermal resistance of heat conduction in the liquid film. Thus, the heat transfer coefficient is strongly dependent on the distribution of the liquid in the tube and, as a consequence, on the flow pattern, which can be influenced by the inclination angle. Fig. 12 shows the heat transfer coefficient as a function of the inclination angle for different vapour qualities and a mass flux of 300 kg/m²s. Fig. 13 is a similar graph for different mass fluxes and a vapour quality of 0.5. At high mass fluxes and high vapour qualities, the heat transfer coefficient is independent of the inclination angle. However, for low mass fluxes and low vapour qualities, the heat transfer coefficient is dependent on the inclination angle. There is an optimum inclination angle that leads to the highest heat transfer coefficient. Depending on experimental conditions, this optimum inclination angle is between -15° and -30° downwards. For low vapour qualities, there is also a specific inclination angle (about 15°) that leads to the lowest heat transfer coefficient for upward flows.

Fig. 12 also shows that for $x = 0.1$ and $G = 300$ kg/m²s, the heat transfer coefficient is increased by about 20% at the optimum inclination angle of about -15° compared with the horizontal orientation. However, the inclination effect depends on the vapour quality and the mass flux and the gain becomes negligible at high vapour qualities and mass fluxes.

Fig. 14 presents a map of the inclination effect on the heat transfer coefficient. The map is drawn on the Thome-El Hajal-Cavallini [19] flow pattern map. The size of the circle represents the inclination effect I , which is defined as the ratio of the difference between the maximum and minimum heat transfer coefficient and the heat transfer coefficient obtained in horizontal orientation:

$$I = \frac{\alpha_{cond,max} - \alpha_{cond,min}}{\alpha_{cond,\beta=0^\circ}} \quad (8)$$

For example, with reference to Fig. 12, for $x = 0.1$ and $G = 300$ kg/m²s, $\alpha_{cond,max} = 2370$ W/m²K (at $\beta = -15^\circ$), $\alpha_{cond,min} = 1570$ W/m²K (at $\beta = -90^\circ$) and $\alpha_{cond,\beta=0^\circ} = 1880$ W/m²K (at $\beta = 0^\circ$). The inclination effect I is equal to 43%.

With this kind of map, we can define a gravity-independent zone where the heat transfer coefficient is independent of the inclination angle (for high x and G), and a gravity-dependent zone where the inclination effect is significant (low x and low G).

The shape of the curves plotted in Fig. 12 and 13 for low vapour qualities and low mass fluxes and especially the presence of minimum and maximum heat transfer coefficient show that the average heat transfer coefficient is the result of several different phenomena, which influence the flow pattern as a function of the inclination angle. Increasing the inclination angle leads to a decrease of the average void fraction in the system because of the gravitational forces that decrease the liquid velocity. This leads to an increase of the liquid film conduction resistance in the system and thus to a decrease of the heat transfer coefficient. For $G = 300$ kg/m²s and for low vapour qualities ($x = 0.1$ and $x = 0.25$),

we observed a plug and slug flow pattern for slightly inclined upward flows. For sharper inclination angles, the flow is more and more turbulent and churn flow pattern appears. Churn flow leads to a better heat transfer coefficient than plug and slug flows because of the instabilities that increase the heat transfer.

For slightly downward flows, the gravitational forces lead to an increase in the liquid velocity and thus to an increase of the void fraction: the flow becomes stratified. The stratified flow pattern leads to the highest heat transfer coefficient because of the presence of the liquid film at the top of the tube. The more the tube is inclined, the thinner the liquid film is at the bottom of the tube and the higher the heat transfer coefficient is. However, the more the tube is inclined, the more the liquid-vapour interface is curved. This leads to an increase of the wetted perimeter at the bottom of the tube.

Beyond a certain inclination angle, the heat transfer coefficient decreases because of the decrease of the perimeter occupied by the thin film of condensation at the top of the tube, where most of the condensation occurs. This is highlighted in Fig. 15, which shows flow patterns and heat transfer coefficients for $x = 0.1$ and $G = 300 \text{ kg/m}^2\text{s}$ and for $x = 0.25$ and $G = 200 \text{ kg/m}^2\text{s}$ for downward orientations. A minimum in the wetted perimeter can be observed for an angle of about 45° for both cases. It does not correspond exactly to a maximum for the heat transfer coefficient, which means that the thickness of the condensation film at the top of the tube is also affected by the inclination angle. The heat transfer coefficient mainly depends on the perimeter occupied by the condensation film and its thickness. For vertical downward orientation, we observed churn flows, which leads to low heat transfer coefficients compared with stratified flows.

In conclusion, the prediction of the heat transfer coefficients for condensing flows in inclined tubes requires a mechanistic model to predict the flow patterns. Then, specific models have to be developed, which depend on the flow pattern. For annular flows, the heat transfer coefficient is not dependent on the inclination angle but for stratified flows, it is important to take into account the inclination effect on the liquid distribution around the perimeter of the tube: three major parameters were highlighted in this study: the void fraction, the curvature of the liquid-vapour interface and the condensation film thickness.

6. Conclusions

Convective condensation experiments were conducted in a smooth inclined tube for the whole range of inclination angles from vertical downward flow to vertical upward flow. R134a at a saturation temperature of 40°C was used, mass fluxes and vapour qualities ranging from 200 to $600 \text{ kg/m}^2\text{s}$ and 0.1 to 0.9 respectively.

The inclination effect on the flow pattern and heat transfer coefficient was studied. The distribution of the fluids in the tube is the result of a balance between gravitational, shear and capillary forces. It appears that the inclination angle has a strong effect on the liquid distribution in the tube and

thus affects the flow patterns and the condensation heat transfer coefficients. An optimal inclination angle that leads to the highest heat transfer coefficient can be found: the increase of heat transfer can be up to 20% for an inclination angle of -15° (downward flow) but the heat transfer coefficient can also be decreased for upward flows. For high mass fluxes and high vapour qualities, the shear forces are predominant: the flow remains annular and the condensation heat transfer coefficient is constant, whatever the angle of inclination.

A comparison of the flow patterns of this study were made with two models available in the literature. It shows that none of them is able to predict correctly the flow pattern transitions for R134a condensing in an inclined 8.38 mm inner diameter smooth tube. It was also shown that the heat transfer coefficient is closely dependent on the flow pattern. These results highlight the necessity to develop new predictive tools, in terms of flow pattern maps and heat transfer correlations, to try to optimise the heat transfer in industrial processes just by inclining the condenser tubes. However, more experimental studies are required to fully understand the different phenomena that influence convective condensation in inclined tubes.

Acknowledgements

The funding obtained from the NRF, TESP, University of Stellenbosch/University of Pretoria, SANERI/SANEDI, CSIR, EEDSM Hub and NAC is acknowledged and duly appreciated.

References

- [1] A. Cavallini, G. Censi, D. Del Col, L. Doretti, G.A. Longo, L. Rossetto, et al., Condensation inside and outside smooth and enhanced tubes - a review of recent research, *Int. J. Refrig.* 26 (2003) 373-392.
- [2] L. Liebenberg, J.P. Meyer, A review of flow pattern-based predictive correlations during refrigerant condensation in horizontally smooth and enhanced tubes, *Heat Transfer Eng.* 29 (2008) 3-19.
- [3] A. Miyara, Condensation of hydrocarbons - A review, *Int. J. Refrig.* 31 (2008) 621-632.
- [4] A.S. Dalkilic, S. Wongwises, Intensive literature review of condensation inside smooth and enhanced tubes, *Int. J. Heat Mass Transfer.* 52 (2009) 3409-3426.
- [5] S. Lips, J.P. Meyer, Two-phase flow in inclined tubes with specific reference to condensation: A review, *Int. J. Multiphase Flow.* 37 (2011) 845-859.
- [6] J.C.Y. Wang, Y. Ma, Condensation heat transfer inside vertical and inclined thermosyphons, *J. Heat Transfer.* 113 (1991) 777-780.
- [7] S.H. Noie, M.R.S. Emami, M. Khoshnoodi, Effect of inclination angle and filling ratio on thermal performance of a two-phase closed thermosyphon under normal operating conditions, *Heat Transfer Eng.* 28 (2007) 365.
- [8] J.C. Chato, Laminar condensation inside horizontal and inclined tubes, Massachusetts Institute of Technology, 1960.
- [9] B.-X. Wang, X.-Z. Du, Study on laminar film-wise condensation for vapor flow in an inclined small/mini-diameter tube, *Int. J. Heat Mass Transfer.* 43 (2000) 1859-1868.
- [10] R. Würfel, T. Kreutzer, W. Fratzscher, Turbulence transfer processes in adiabatic and

- condensing film flow in an inclined tube, *Chem. Eng. Technol.* 26 (2003) 439-448.
- [11] M.A. Akhavan-Behabadi, R. Kumar, S.G. Mohseni, Condensation heat transfer of R-134a inside a microfin tube with different tube inclinations, *Int. J. Heat Mass Transfer.* 50 (2007) 4864-4871.
- [12] T. Nitheanandan, H.M. Soliman, Influence of tube inclination on the flow regime boundaries of condensing steam, *Can. J. Chem. Eng.* 71 (1993) 35-41.
- [13] T. Nitheanandan, H.M. Soliman, Analysis of the stratified/nonstratified transitional boundary in horizontal and slightly inclined condensing flows, *Can. J. Chem. Eng.* 72 (1994) 26-34.
- [14] W.C. Wang, X.H. Ma, Z.D. Wei, P. Yu, Two-phase flow patterns and transition characteristics for in-tube condensation with different surface inclinations, *Int. J. Heat Mass Transfer.* 41 (1998) 4341-4349.
- [15] S. Lips, J.P. Meyer, Experimental study of convective condensation in an inclined smooth tube. Part II: Inclination effect on pressure drop and void fraction, *Int. J. Heat Mass Transfer.* (2011) Submitted for review.
- [16] E. van Rooyen, M. Christians, L. Liebenberg, J.P. Meyer, Probabilistic flow pattern-based heat transfer correlation for condensing intermittent flow of refrigerants in smooth horizontal tubes, *Int. J. Heat Mass Transfer.* 53 (2010) 1446-1460.
- [17] R. Suliman, L. Liebenberg, J.P. Meyer, Improved flow pattern map for accurate prediction of the heat transfer coefficients during condensation of R-134a in smooth horizontal tubes and within the low-mass flux range, *Int. J. Heat Mass Transfer.* 52 (2009) 5701-5711.
- [18] REFPROP, NIST thermodynamic properties of refrigerants and refrigerant mixtures (REFPROP), Version 8.0, NIST Standard Reference Database 23, National Institute of Standards and Technology, Gaithersburg, MD, 2005.
- [19] J. El Hajal, J.R. Thome, A. Cavallini, Condensation in horizontal tubes. Part 1: two-phase flow pattern map, *Int. J. Heat Mass Transfer.* 46 (2003) 3349-3363.
- [20] D. Kim, A.J. Ghajar, Heat transfer measurements and correlations for air-water flow of different flow patterns in a horizontal pipe, *Exp. Therm. Fluid Sci.* 25 (2002) 659-676.
- [21] D. Barnea, A unified model for predicting flow-pattern transitions for the whole range of pipe inclinations, *Int. J. Multiphase Flow.* 13 (1987) 1-12.
- [22] J. Weisman, S.Y. Kang, Flow pattern transitions in vertical and upwardly inclined lines, *Int. J. Multiphase Flow.* 7 (1981) 271-291.
- [23] T.J. Crawford, C.B. Weinberger, J. Weisman, Two-phase flow patterns and void fractions in downward flow. Part I: steady-state flow patterns, *Int. J. Multiphase Flow.* 11 (1985) 761-782.
- [24] J.R. Thome, J. El Hajal, A. Cavallini, Condensation in horizontal tubes. Part 2: new heat transfer model based on flow regimes, *Int. J. Heat Mass Transfer.* 46 (2003) 3365-3387.
- [25] A. Cavallini, D. Del Col, L. Doretti, M. Matkovic, L. Rossetto, C. Zilio, et al., Condensation in horizontal smooth tubes: a new heat transfer model for heat exchanger design, *Heat Transfer Eng.* 27 (2006) 31-38.
- [26] M.M. Shah, A general correlation for heat transfer during film condensation inside pipes, *Int. J. Heat Mass Transfer.* 22 (1979) 547-556.
- [27] M.K. Dobson, J.C. Chato, Condensation in smooth horizontal tubes, *J. Heat Transfer.* 120 (1998) 193.

List of figure captions

- Fig. 1.** Schematic diagram of the experimental set-up (EEV = electronic expansion valve).
- Fig. 2.** Experimental test points on the Thome-El Hajal-Cavallini [19] flow pattern map (R134a; $d_i = 8.38$ mm; $T_{\text{sat}} = 40^\circ\text{C}$).
- Fig. 3.** The different types of flow patterns considered in this study (R134a, the time length of the sequence is 0.15 s).
- Fig. 4.** Effect of the inclination angle on the flow pattern for different vapour qualities (R134a, $G = 300$ kg/m²s).
- Fig. 5.** Effect of the inclination angle on the flow pattern for different mass fluxes (R134a, $x = 0.5$).
- Fig. 6.** Comparison of experimental flow patterns for the horizontal orientation with the Thome-El Hajal-Cavallini flow pattern map [19]; (a)-(f) refer to the flow patterns in Fig. 4 at an inclination angle of 0° and a mass flux of 300 kg/m²s.
- Fig. 7.** Comparison of experimental flow patterns with the Barnea [21] flow pattern map (An = Annular, I = Intermittent, S = Stratified).
- Fig. 8.** Comparison of experimental flow patterns with the Crawford et al. [22,23] flow pattern map (An = Annular, B = Bubbly, I = Intermittent, S = Stratified).
- Fig. 9.** Experimental heat transfer results for horizontal orientation compared with the correlations of Thome et al. [24], Cavallini et al. [25] and Shah [26].
- Fig. 10.** A comparison between the experimental heat transfer results and different correlations for vertical upward flow.
- Fig. 11.** A comparison between the experimental heat transfer results and different correlations for vertical downward flow.
- Fig. 12.** Inclination effect on heat transfer coefficients for different vapour qualities ($G = 300$ kg/m²s).
- Fig. 13.** Inclination effect on heat transfer coefficients for different mass fluxes ($x = 0.5$).
- Fig. 14.** Map of the inclination effect on heat transfer coefficients drawn on the Thome-El Hajal-Cavallini [19] flow pattern map.
- Fig. 15.** Flow patterns and heat transfer coefficients for downward flows at low mass fluxes and low vapour qualities.

List of table captions

Table 1 Range of experimental parameters and fluctuations.

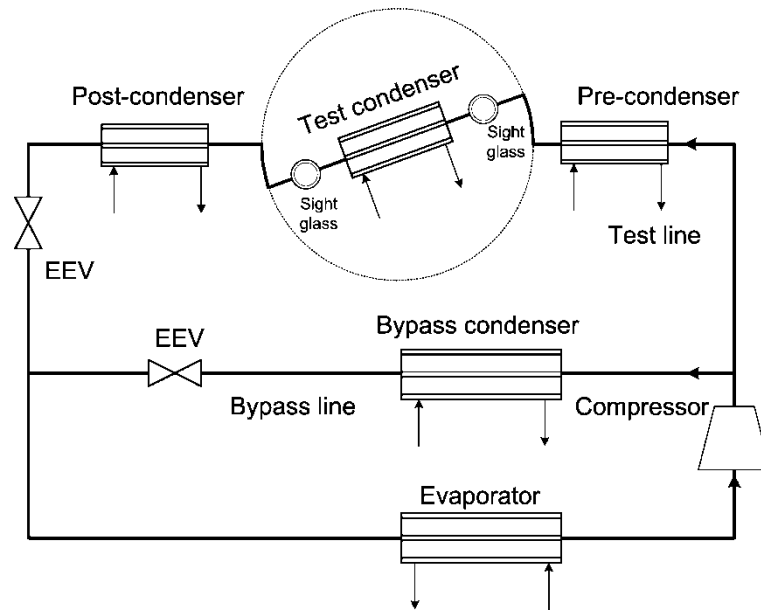


Fig. 1. Schematic diagram of the experimental set-up (EEV = electronic expansion valve).

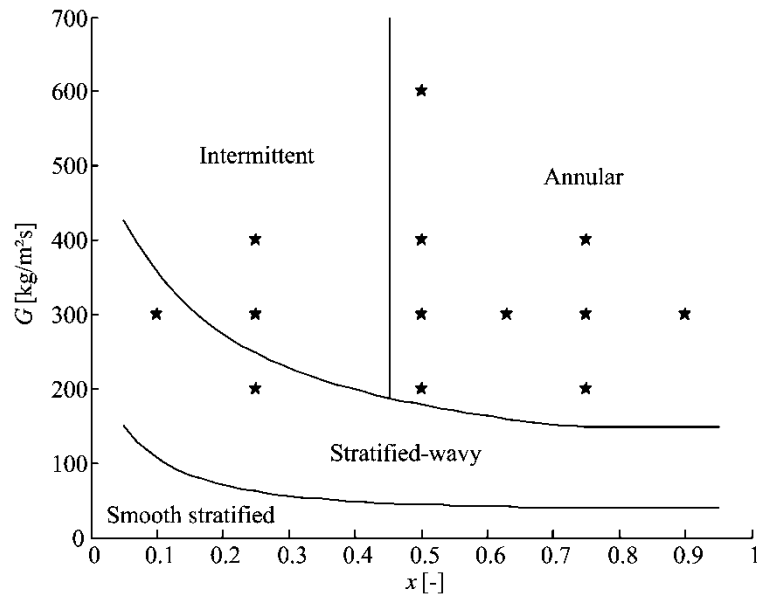


Fig. 2. Experimental test points on the Thome-El Hajal-Cavallini [19] flow pattern map (R134a; $d_i = 8.38$ mm; $T_{\text{sat}} = 40^\circ\text{C}$).

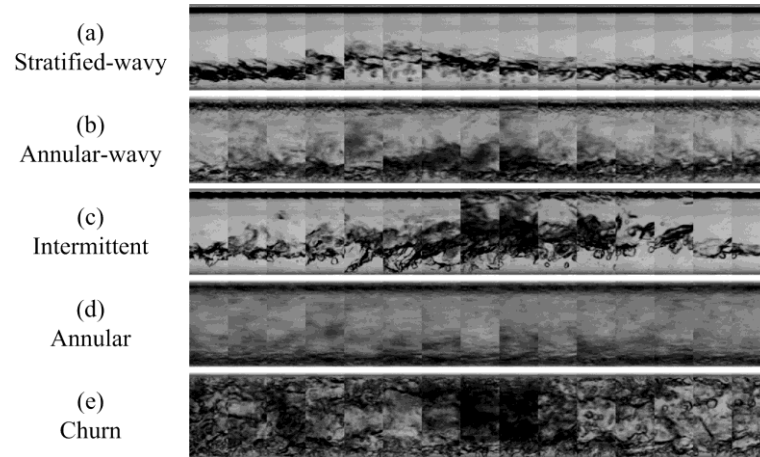


Fig. 3. The different types of flow patterns considered in this study (R134a, the time length of the sequence is 0.15 s).

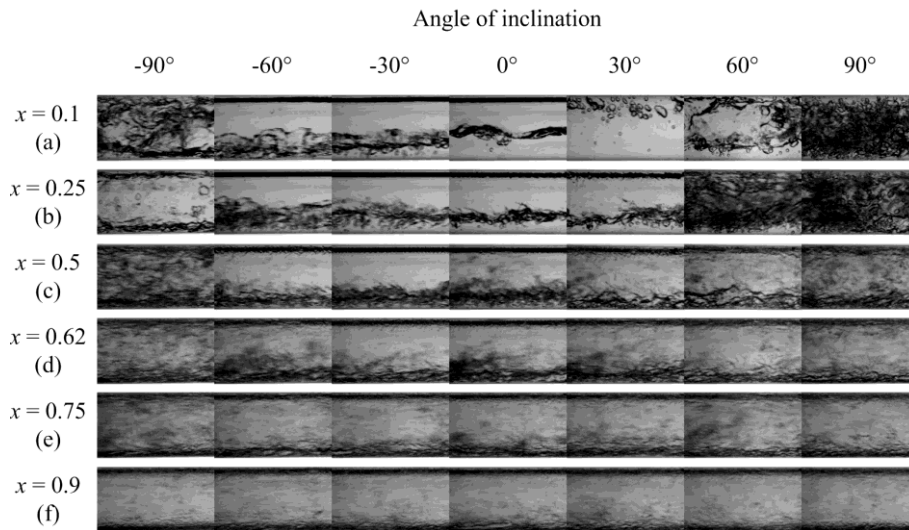


Fig. 4. Effect of the inclination angle on the flow pattern for different vapour qualities (R134a, $G = 300 \text{ kg/m}^2\text{s}$).

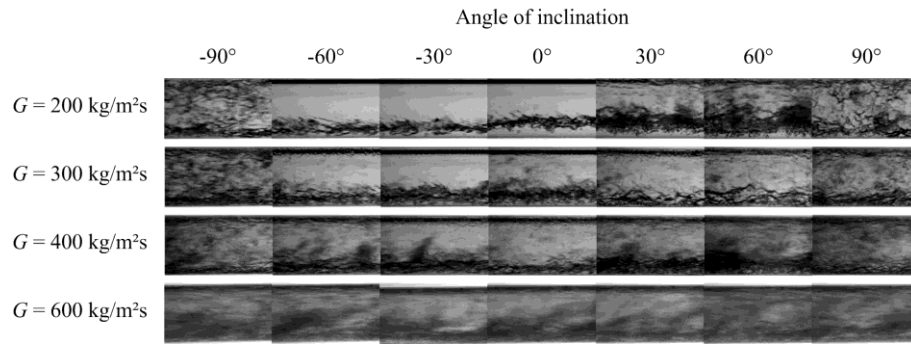


Fig. 5. Effect of the inclination angle on the flow pattern for different mass fluxes (R134a, $x = 0.5$).

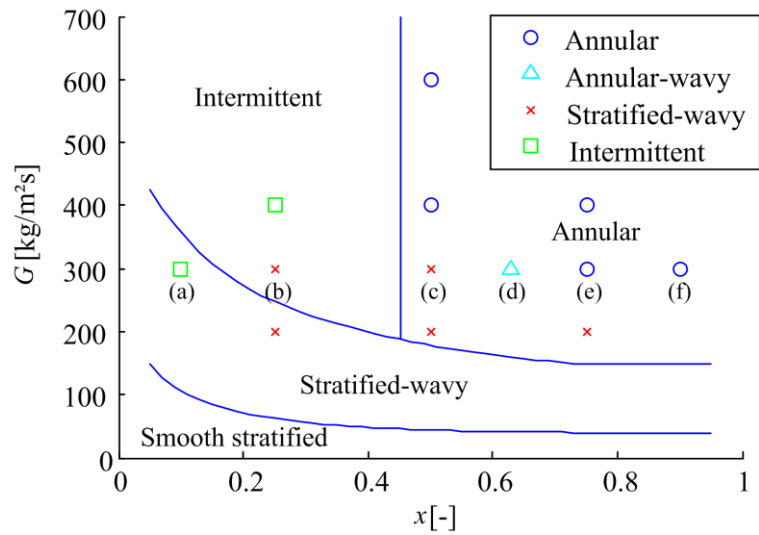


Fig. 6. Comparison of experimental flow patterns for the horizontal orientation with the Thome-El Hajal-Cavallini flow pattern map [19]; (a)-(f) refer to the flow patterns in Fig. 4 at an inclination angle of 0° and a mass flux of $300 \text{ kg/m}^2\text{s}$.

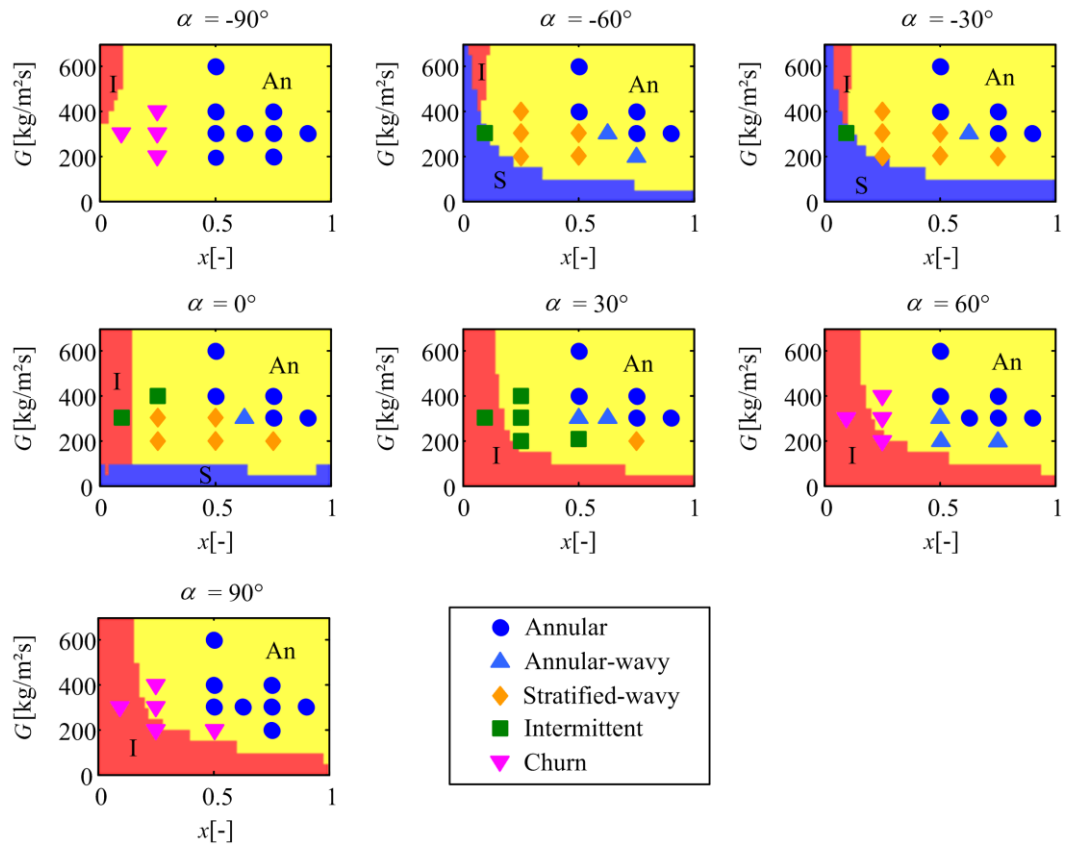


Fig. 7. Comparison of experimental flow patterns with the Barnea [21] flow pattern map (An = Annular, I = Intermittent, S = Stratified).

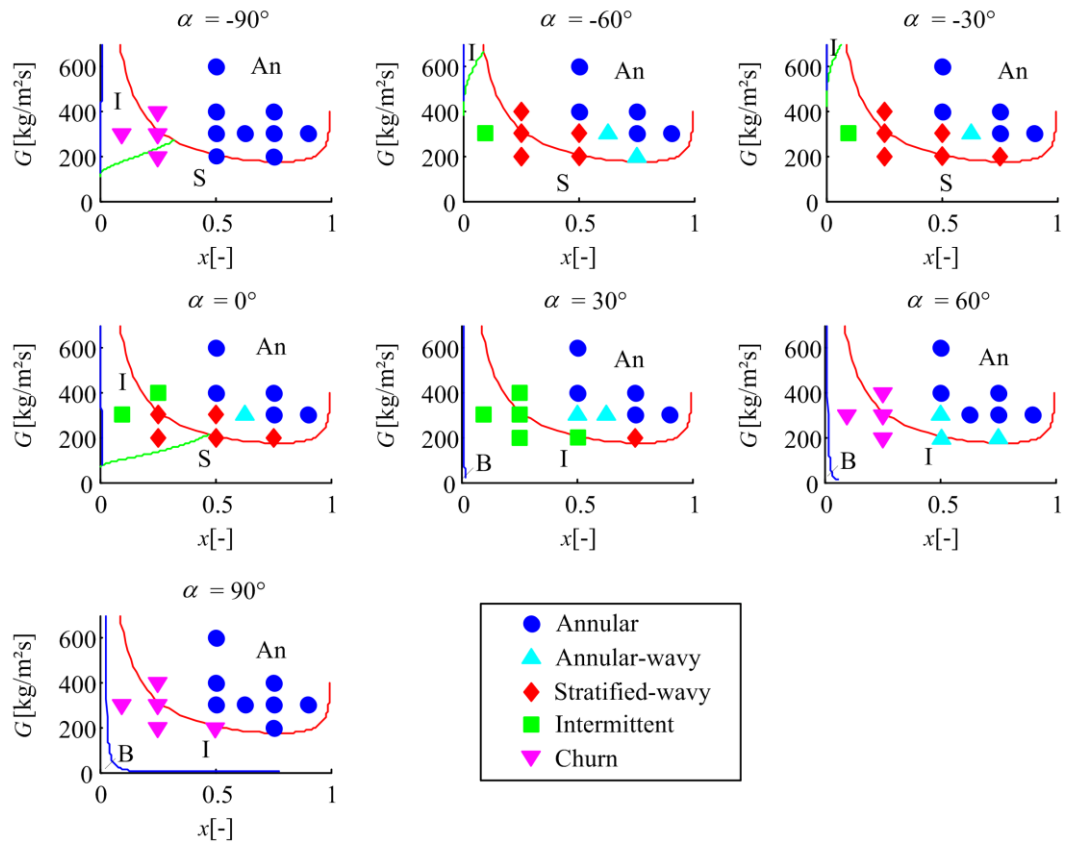


Fig. 8. Comparison of experimental flow patterns with the Crawford et al. [22,23] flow pattern map (An = Annular, B = Bubbly, I = Intermittent, S = Stratified).

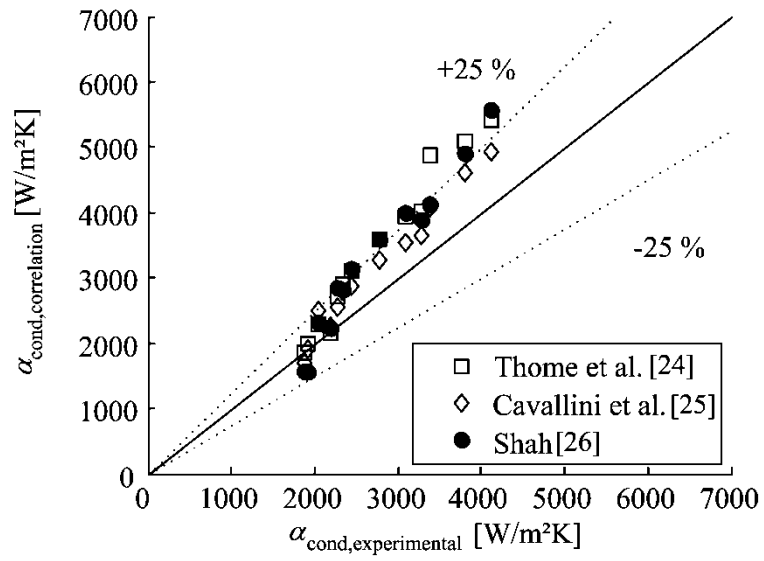


Fig. 9. Experimental heat transfer results for horizontal orientation compared with the correlations of Thome et al. [24], Cavallini et al. [25] and Shah [26].

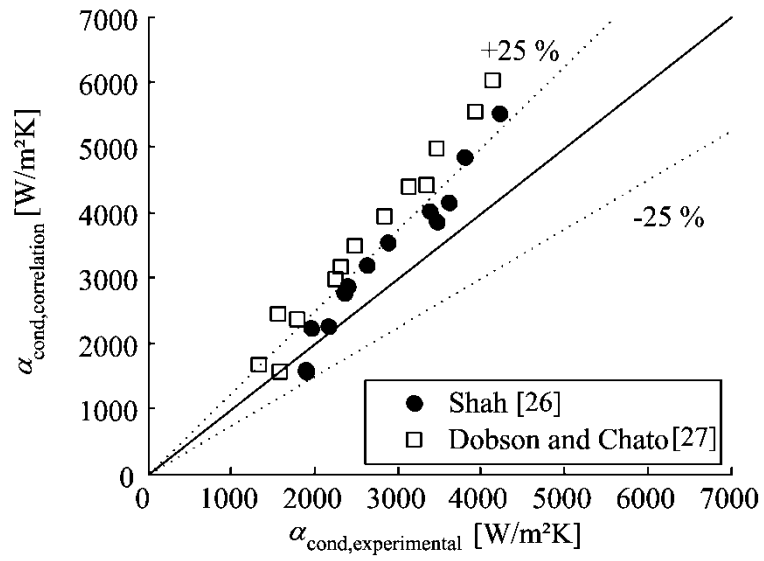


Fig. 10. A comparison between the experimental heat transfer results and different correlations for vertical upward flow.

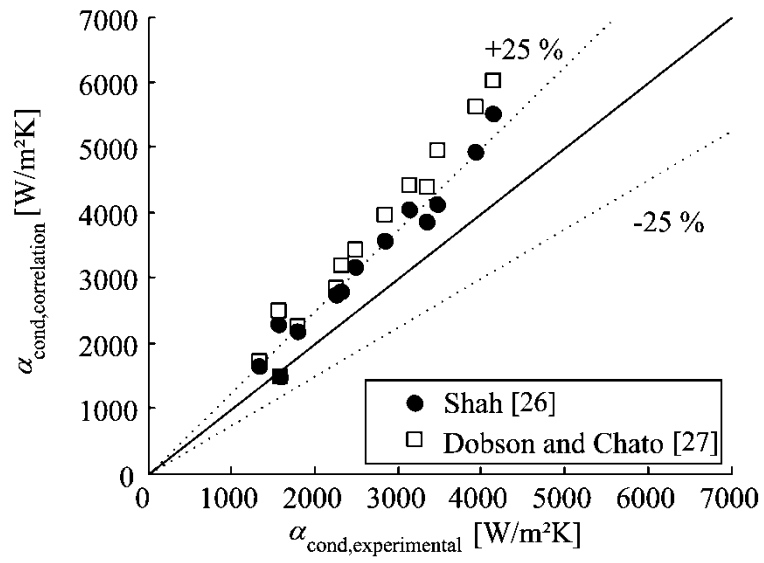


Fig. 11. A comparison between the experimental heat transfer results and different correlations for vertical downward flow.

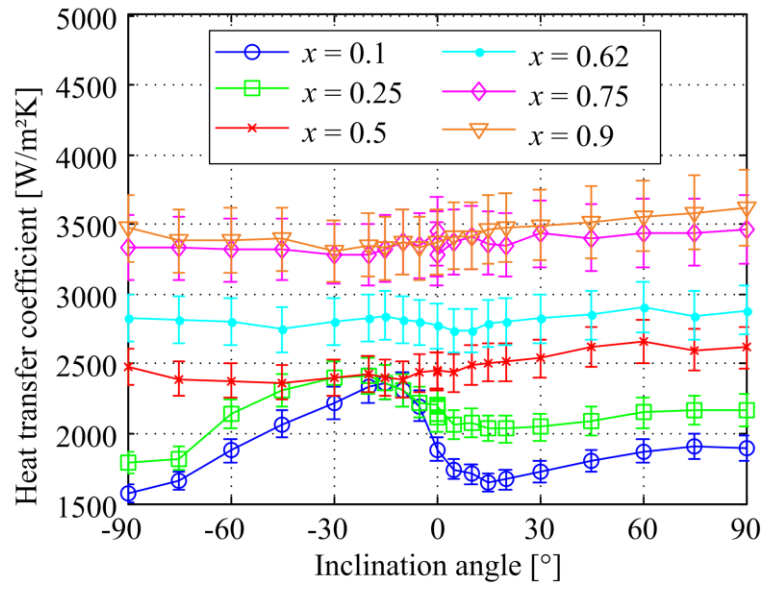


Fig. 12. Inclination effect on heat transfer coefficients for different vapour qualities ($G = 300 \text{ kg/m}^2\text{s}$).

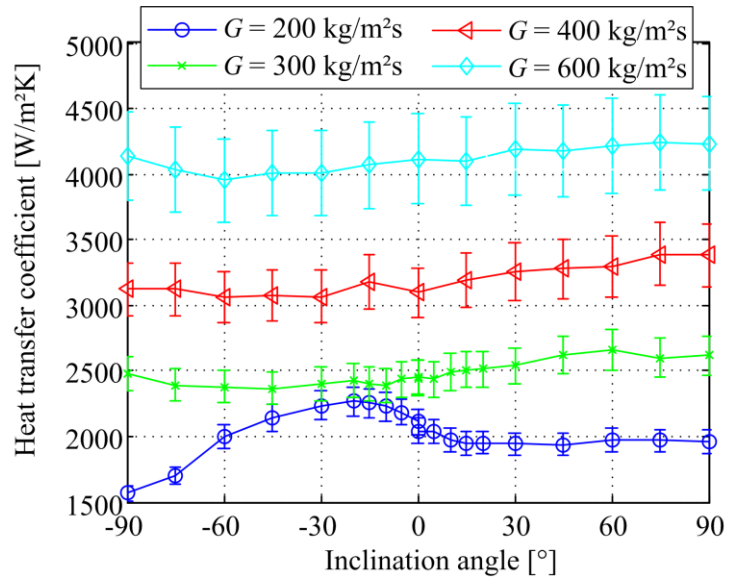


Fig. 13. Inclination effect on heat transfer coefficients for different mass fluxes ($x = 0.5$).

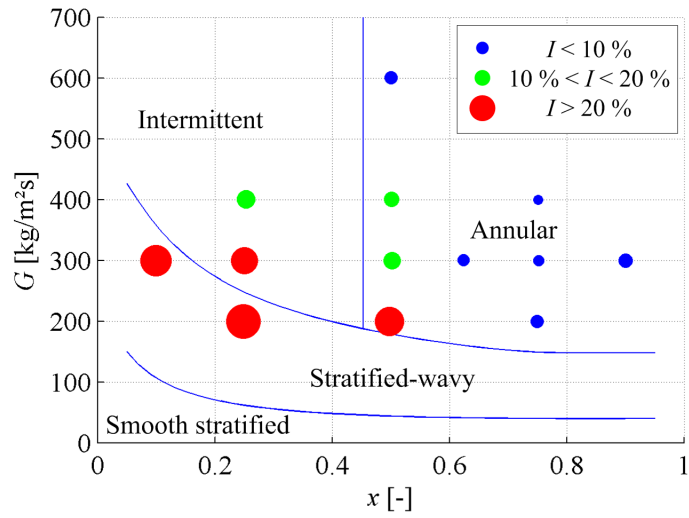


Fig. 14. Map of the inclination effect on heat transfer coefficients drawn on the Thome-El Hajal-Cavallini [19] flow pattern map.

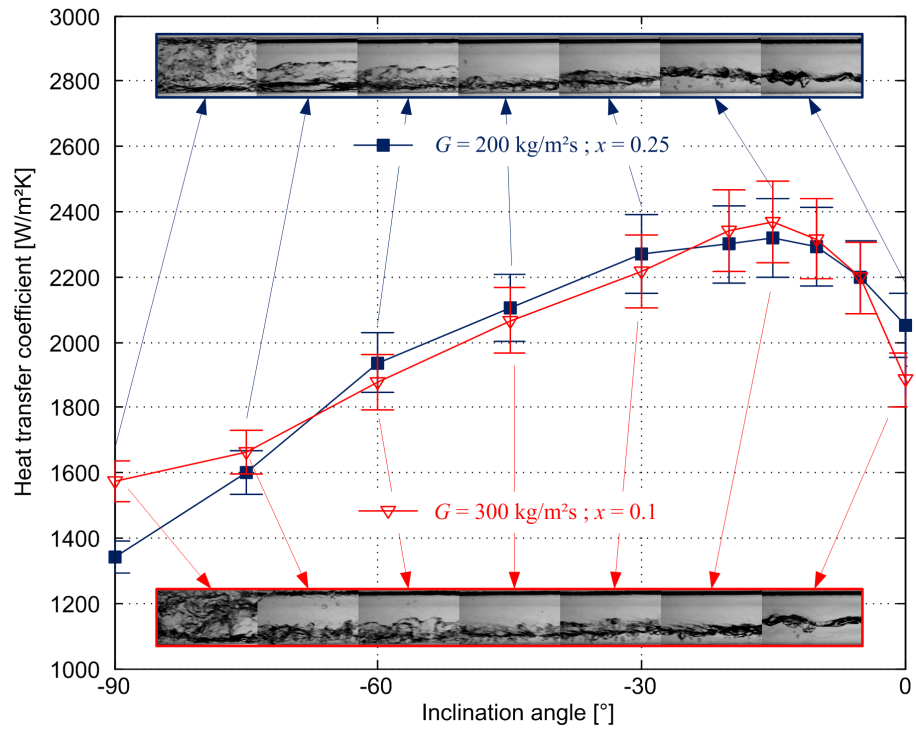


Fig. 15. Flow patterns and heat transfer coefficients for downward flows at low mass fluxes and low vapour qualities.

Table 1

Range of experimental parameters and fluctuations.

Parameter	Range	Fluctuations
T_{sat}	40°C	$\pm 0.5^\circ\text{C}$
G	200-600 kg/m ² s	± 5 kg/m ² s
x	0.1-0.9	± 0.01
Q_{test}	200 W	± 5 W